

## Edge Detection Gives *Chandra* a Sharper View of Cluster Astrophysics

Jeremy Sanders, Stephen Walker,  
John ZuHone, and Elena Bellomi

### Introduction

The X-ray surface brightness of galaxy clusters peaks steeply like a mountain, and like a mountain it can be very hard to see the interesting features on the slopes from far away. Although some clusters can be very pointed, some slightly flat-topped and some with more than one peak because they are merging together, they all have large dynamical ranges in surface brightness from the faint outskirts to the bright central region. The intracluster medium, which is the hot atmosphere that fills clusters and accounts for most of their baryons, generates the X-ray emission. The X-ray emission is sensitive to the density-squared of this material, meaning the X-ray brightness grows steeply as the density increases towards the center.

Because of this sensitivity to density, studying the X-ray emission provides vital clues to understand what physical processes are taking place in clusters. Feedback by active galactic nuclei, sloshing of gas in the potential well of the system, and mergers all affect the gas density. The issue is that the scale of these variations is often relatively small compared to the peak as a whole. While major mergers, like the Bullet cluster, are easy to see directly in an X-ray image, simulations of clusters show we should expect a lot of structure on small scales (a few kpc) in all clusters, particularly if turbulence or fluid instabilities are present. This problem is compounded when viewing images of clusters on media with limited dynamic range.

### Structure-Finding Methods for Imaging

A common way to remove the peak and see the interesting edges, filaments, cavities or ripples is to model the cluster emission, then subtract or divide the X-ray image or surface brightness profile by the model. This often works well, but real clusters are not spherical beta models (note that a beta model is a common parameterization for the X-ray surface brightness with a flat core and a powerlaw at larger radii, although this is not what the average cluster looks like—see Sanders et al. 2018). The model can either be too crude to account for most of the cluster emission, or inappropriate modeling can introduce structure that is not present and can also remove interesting features by over-modeling.

After the launch of *Chandra* with its high spatial resolution imaging, the problem became acute. This led to the use of image processing techniques, such as unsharp masking, being applied to *Chandra* data. Unsharp masking has a long

history of being applied to astronomical data. David Malin, in particular, is famous for applying it to photographic astronomical images (Malin & Zealey 1979). When used in X-ray astronomy, the typical observer smooths their image by a Gaussian with a particular length scale and subtracts or divides this from the image smoothed by a smaller or no Gaussian. In this way, large scale fluctuations are removed to reveal the small scale features in the data. This technique has, for example, uncovered the ripple-like structures in the Perseus cluster (Fabian et al. 2003). Unsharp masking is a simple but powerful technique and is well suited for detecting compact single-scale features. It does not work as well for elongated linear structures.

Other forms of structure detection in clusters have included wavelet decomposition, which decomposes images into various scales (e.g., Grebenev et al. 1995). If the emission you are interested in has a dominating scale, wavelets are a good choice to search for such structure. We have also investigated filtering out large scales in the spatial frequency domain with success (Sanders & Fabian 2008), although care has to be taken that aliasing and the frequency wings of bright sources do not introduce spurious features.

### The Gaussian Gradient Magnitude (GGM) Filter

Working on a deep *Chandra* observation of the Centaurus cluster (Sanders et al. 2016a), it was suggested by Katherine Blundell to try out the Sobel filter on our high quality X-ray data, to highlight the edges in the surface brightness. The Sobel filter or operator is a simple convolution with a 3×3 matrix which measures the pixel-scale gradient in the image it is applied to in one direction. The Sobel filter has been used in radio astronomy previously to highlight edges in jets (e.g., Laing et al. 2013). In addition, edge filters have also been applied when analyzing cluster simulations (Roediger et al. 2013), but we are not aware of applications on X-ray data. Edge detection also has a long history in computer vision applications. We discovered with further experimentation that a more advanced version of a gradient filter, the Gaussian Gradient Magnitude (GGM), was an excellent tool for revealing edges in cluster images. In this filter, the image is convolved with a function which is the gradient of a Gaussian in either the X or Y directions with a particular size scale, measuring the gradients on this scale. The two gradient images can then be used to compute the gradient magnitude for that scale.

Measuring surface brightness gradients is optimal for cluster studies because many of the physical processes in clusters create edges or shells which lead to strong gradients. For example, a cold front is a discontinuity in temperature and density thought to be generated by sloshing of the intracluster medium in the potential well of a cluster caused by an interloper which disturbs that well (Markevitch & Vikhlinin 2007). Another example is a shock, perhaps generated by a merger or AGN outburst, that can be seen via

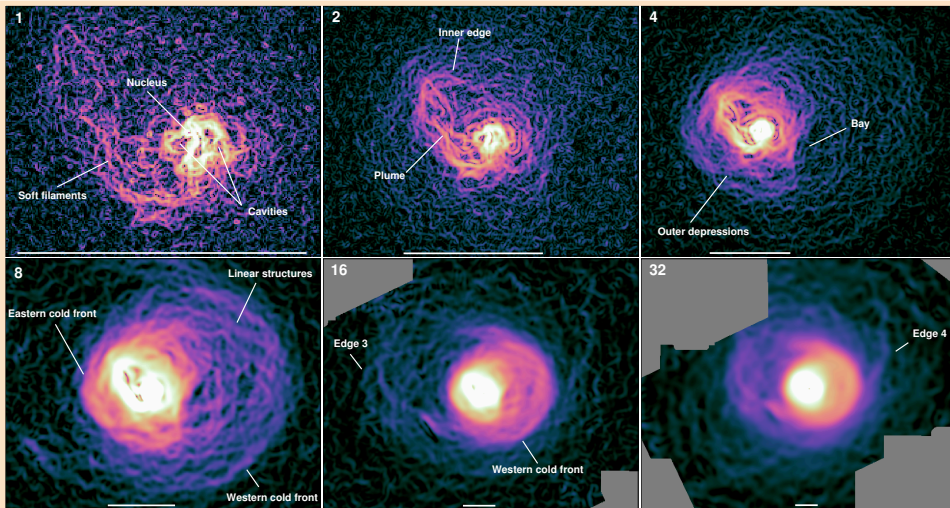


Figure 1: Images of the Centaurus cluster with the gradient measured on scales increasing by a factor of two, in units of one  $\frac{1}{2}$  arcsec pixel (north is up, and east is left). The white bars show 20 kpc in each panel. Adapted from Sanders et al. (2016a).

its density jump. *Chandra* has revealed that cavities, filled with relativistic bubbles generated by the central AGN, are an almost ubiquitous feature of clusters with short central cooling times.

We applied the GGM technique to very deep *Chandra* X-ray images of the Centaurus cluster. Centaurus is a nearby ( $z \sim 0.01$ ) X-ray bright galaxy cluster. Several physical processes are occurring within the cluster; the main subcluster is merging with another 200 kpc away, the core shows clear evidence for episodic AGN outbursts and contains some of the clearest examples of cold fronts in the universe.

Figure 1 shows filtered images of the Centaurus cluster, with filtering scales increasing by factors of two, after masking out point sources. In the image, high-gradient regions, or edges, are represented by bright colors while dark colors show the low-gradient regions. There are two cavities which lie either side of the nucleus in the center and in the smallest-scale image we see their sharp edges. These cavities are filled by AGN-outburst generated bubbles of relativistic plasma seen by its radio emission. These bubbles are weakly shocking their surroundings when examined with detailed spatially resolved spectroscopy. There is a plume of soft filamentary emission, first seen in early *Chandra* observations of this object (Sanders & Fabian 2002), that we suggest is caused by cooler material lifted out from the core of the cluster in the wake of a buoyantly rising bubble of plasma, whose edge seen in Panel “2” (labeled “Inner edge”). There is also low frequency radio emission seen inside this region, supporting this origin (Figure 3 bottom right). We also see evidence for a number of edges associated with depressions, labeled “Outer depressions”. We interpret these as caused by bubbles from old episodes of AGN outbursts, as there is also low frequency radio emission associated with them in the opposite direction of the plume. In panel “8” there are a number of

linear structures. We hypothesize these could be sound waves generated by outbursts of the AGN. In that case their wavelength implies a period of around 6 Myr. Alternative explanations include Kelvin-Helmholtz instabilities (KHI) or magnetic field structures. On larger scales are the two cold fronts, “Eastern cold front”, in panel “8” and one the western one at larger radius (“Western cold front” in panels “8” and “16”). There are also two further possible cold fronts, labeled Edge 3 and Edge 4.

Not all of the structure revealed by the GGM filtering technique in the images is real. Poisson noise in these filtered images has a peculiar “wormy” nature, so care should be taken that the features are real and not due to noise (see “Assessing the significance of features” on page 3).

For visual purposes it is useful to combine together images filtered on different scales. This is important in the outskirts of the cluster where the count density is too low to measure the gradient. We developed a simple technique to add images filtered on different scales using a radial weighting function. With the aid of a graphical user interface we can interactively adjust the weighting to highlight the significant edges in the image while reducing the noise-related artifacts from low count density regions.

Figure 2 shows our combined filtered image of M87 in the center of the Virgo cluster, combining 1Ms of *Chandra*

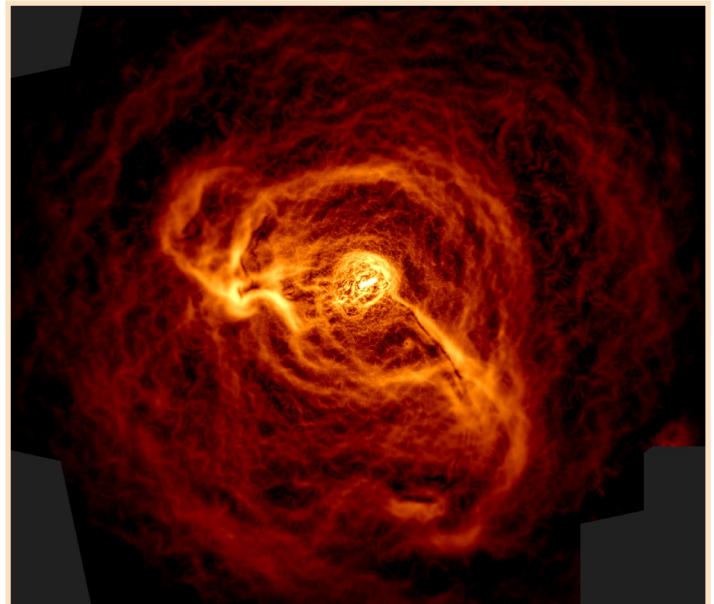


Figure 2: Multi-scale filtered X-ray image of M87 in the center of the Virgo cluster. Created by radially combining filtered images with scales of 1 to 32  $\frac{1}{2}$  arcsec pixels. The image measures 80 kpc across.

data. The combined filtered image allows us to display a great deal of structure in a single image. The image covers the jet in the central region (Marshall et al. 2002), the surrounding cavities generated by a cocoon of relativistic plasma (Young et al. 2002), the well known arms of soft X-ray emission interacting with the radio source (Forman et al. 2007), and the circular structure of  $\sim 14$  kpc radius from a weak shock generated an outburst of the central AGN (Forman et al. 2007).

Gradient filtering is particularly well-suited for uncovering edges in imaging of clusters, while unsharp masking is perhaps a better choice to identify spatially compact clumps or cavities. Many of the structures in clusters, for example cold fronts, cavity edges, shocks, are edge-like in nature, so gradient filtering is an excellent choice to find them.

### Science Discoveries: A Kelvin-Helmholtz Instability (KHI) in the Sloshing Cold Front of the Perseus Cluster

Deep *Chandra* observations of nearby galaxy clusters, (namely the Perseus cluster, the Centaurus cluster, and Abell 1795) have revealed unusual concave surface brightness edges referred to as “bays”. Walker et al. (2017) explored the various possible formation scenarios for these bays, by combining X-ray and deep radio observations and comparing these observations to simulations of gas sloshing. We found that these bays cannot be simply explained by AGN feedback activity or standard convex sloshing cold fronts (Figure 3).

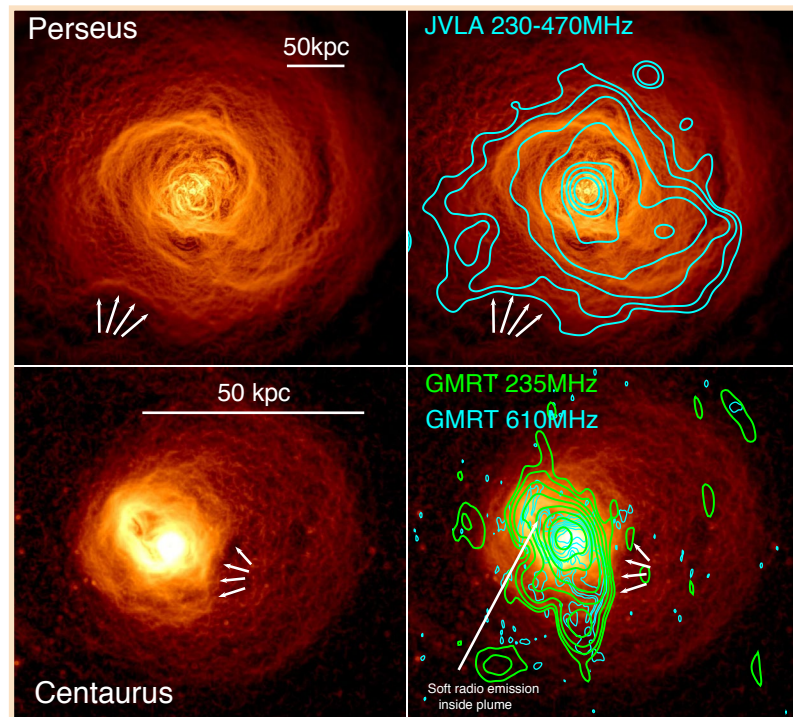


Figure 3. The left column shows multi-scale GGM filtered images of the Perseus cluster (top) and the Centaurus cluster (bottom). In the right hand column, radio contours are overlaid which appear to be constrained behind the concave ‘bay’ features. Adapted from Walker et al. (2017).

### Assessing the significance of features

Although gradient filtering is a great tool to find structures, care must be taken to ensure features are robust. As we see in Figure 1, the noise in filtered images has a peculiar linear structure, unlike normal intensity images. Typically the filamentary features lie along surface brightness contours. For a fixed filtering scale, the noise increases towards regions with lower surface brightness. There are a number of methods to check for significance. These include examining the original unfiltered image in detail, for example by blinking between the original and the filtered image, making surface brightness profiles across a structure and looking at filtered model images fitted to the original image. Optimization of the position-dependent length scales used in gradient filtering to improve significance and reduce the noise is a current area of research.

We eliminated AGN feedback activity as an explanation because the bays are often one-sided, whereas AGN inflated cavities are often double-sided and correlated with jets launched by the central AGN.

Comparing to models of empty cavities in the intracluster medium, the observed surface brightness drop is too small, while the observed temperature jump is too large. If we try to increase the temperature jump in the cavity model by assuming a cavity which is highly elongated along the line of sight, the discrepancy between the surface brightness profiles becomes even larger. No geometry of cavity is able to reproduce the observations. Across the bay edge the temperature increases as the density decreases (on scales of the order of the Coulomb mean free path), similar to cold fronts, however, bays are concave, while cold fronts are convex.

When we compare observations to sloshing simulations (ZuHone et al. 2011, ZuHone et al. 2016) we find that, for the Perseus cluster, the bay position, size and morphology all bear striking similarity to the large ( $\sim 50$  kpc) KHI that form in these simulations (Figure 4). The magnitudes of the temperature and surface brightness jumps are also in good agreement between the simulations and the observations.

The morphology of the central radio emission in the clusters provides further clues to the nature of the bays. Cavities inflated by AGN are typically filled with radio emission from the diffuse relativistic plasma they contain. Cold fronts on the other hand typically constrain radio halos behind them. When deep radio observations of the central regions of Perseus and Centaurus are overlaid on the X-ray images (Figure 3) we see that the radio contours are confined to regions behind the bays. In Perseus the radio halo has exactly the same concave curvature along the edge of the X-ray bay. This is exactly what would be expected if the bays are concave cold fronts that result from the large KHI such as those predicted by simulations (ZuHone et al. 2011).

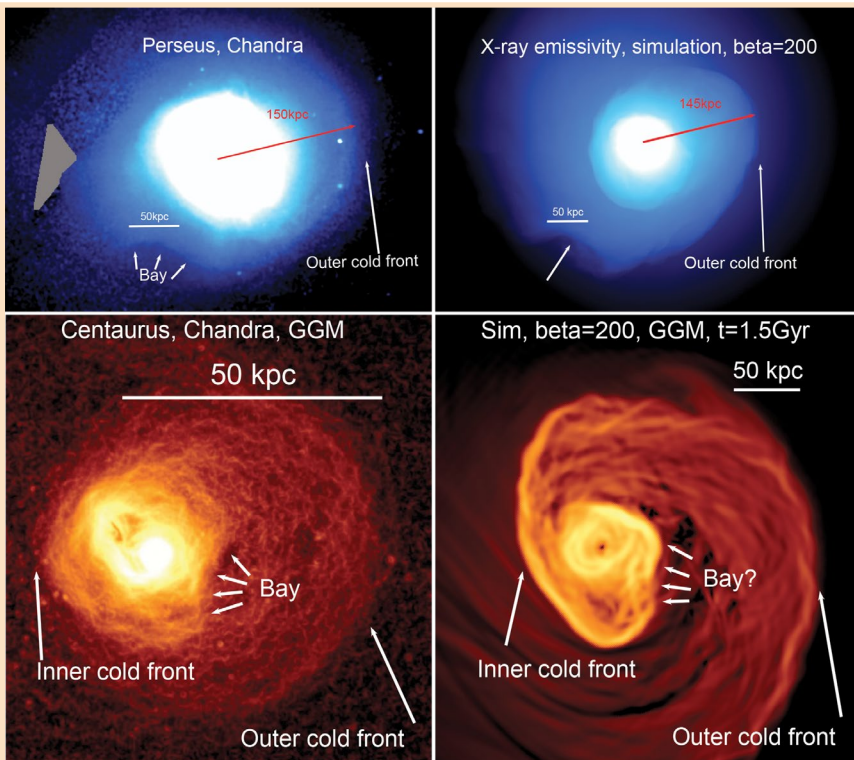


Figure 4: Comparing the locations of the bays in Perseus and Centaurus (left column) with the sloshing simulations from ZuHone et al. 2011 (right column). We are able to find good matches for the bay features in different time epochs of the simulations. Adapted from Walker et al. (2017). Grey triangular region in upper left panel is due to a gap in the coverage of the cluster.

**More Subtle KHI Features in Centaurus and Abell 2142**

When we apply the GGM filter technique to the *Chandra* images of the Centaurus cluster (Sanders et al. 2016a) and Abell 2142 (Walker et al. 2016), shown in Figure 5, we find linear features behind their main cold fronts, (features marked as L1, L2 and L3 for Centaurus, and marked by the white arrows for Abell 2142). These may be evidence for more subtle KHI (Roediger et al. 2011; ZuHone et al. 2011).

**A Quick Way to Map the Width and Jump Ratios Along Cold Fronts.**

As GGM images are maps of the gradient of the X-ray surface brightness, they provide a straightforward way to map variations of the jump ratio and width of cold fronts along their lengths. Typically such measurements require a lengthy process of dividing the cold front into multiple sectors and fitting each sector’s surface brightness profile with a model consisting of a broken powerlaw smoothed by a Gaussian. Applying this technique to Abell 2319 and Abell 3667 (Figure 6, Walker

et al. 2016), we found that the gradient varies along the cold fronts. For A2319 the gradient is highest to the north (position A), and decreases to the south as we move to position B. For A3667, the gradient is highest in the middle of the cold front, and decreases on either side. By comparing to surface brightness profile fitting (Figure 6), we see that for A2319 this gradient decrease occurs because the width of the cold front increases along its length while its jump ratio is constant. By contrast, for A3667, the width is relatively uniform along its length, and the gradient peak in the middle is caused by the jump ratio being higher in the middle of the cold front.

**Edge Detection in Simulations of the Intracluster Medium**

Similar imaging analysis can be applied to simulations of galaxy clusters as well. This opens up the possibilities of using the comparison of the simulated images with the observations to explain the origin of certain edge features (such as the “bays” described above) or discriminating between different physical properties of the ICM. Such comparisons involve producing 2D projections of the X-ray emission expected from 3D hydrodynamic models of the cluster gas from simulations and filtering them

using the GGM technique.

Due to their origin in the relative motion of cold and hot gases in the ICM, cold fronts produced in simulations are associated with strong velocity shears, making them susceptible to the effects of KHI. KHI can be suppressed, to a degree, by viscosity or magnetic tension, implying that the properties of KHI in observed cold fronts can place constraints on these properties of the cluster plasma.

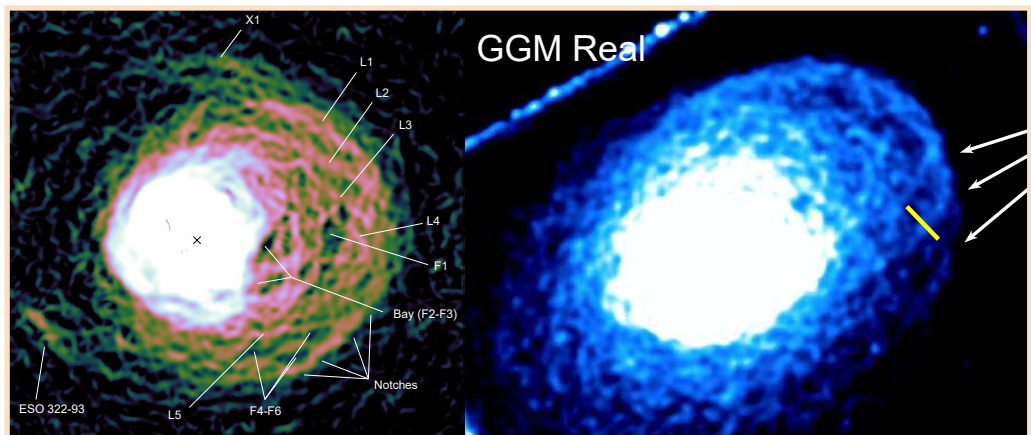


Figure 5. GGM filtered images of Centaurus (left from Sanders et al. 2016a) and Abell 2142 (right). We find linear features behind the cold front highlighted by the white arrows (features L1, L2 and L3 for Centaurus), which may be evidence of subtle KHI rolls. See Sanders et al. (2016a) for discussion of the notches indicated in the image of Centaurus (left). X-ray surface brightness profiles of ripples along the yellow line (in right panel) are studied further in Walker et al. (2016).

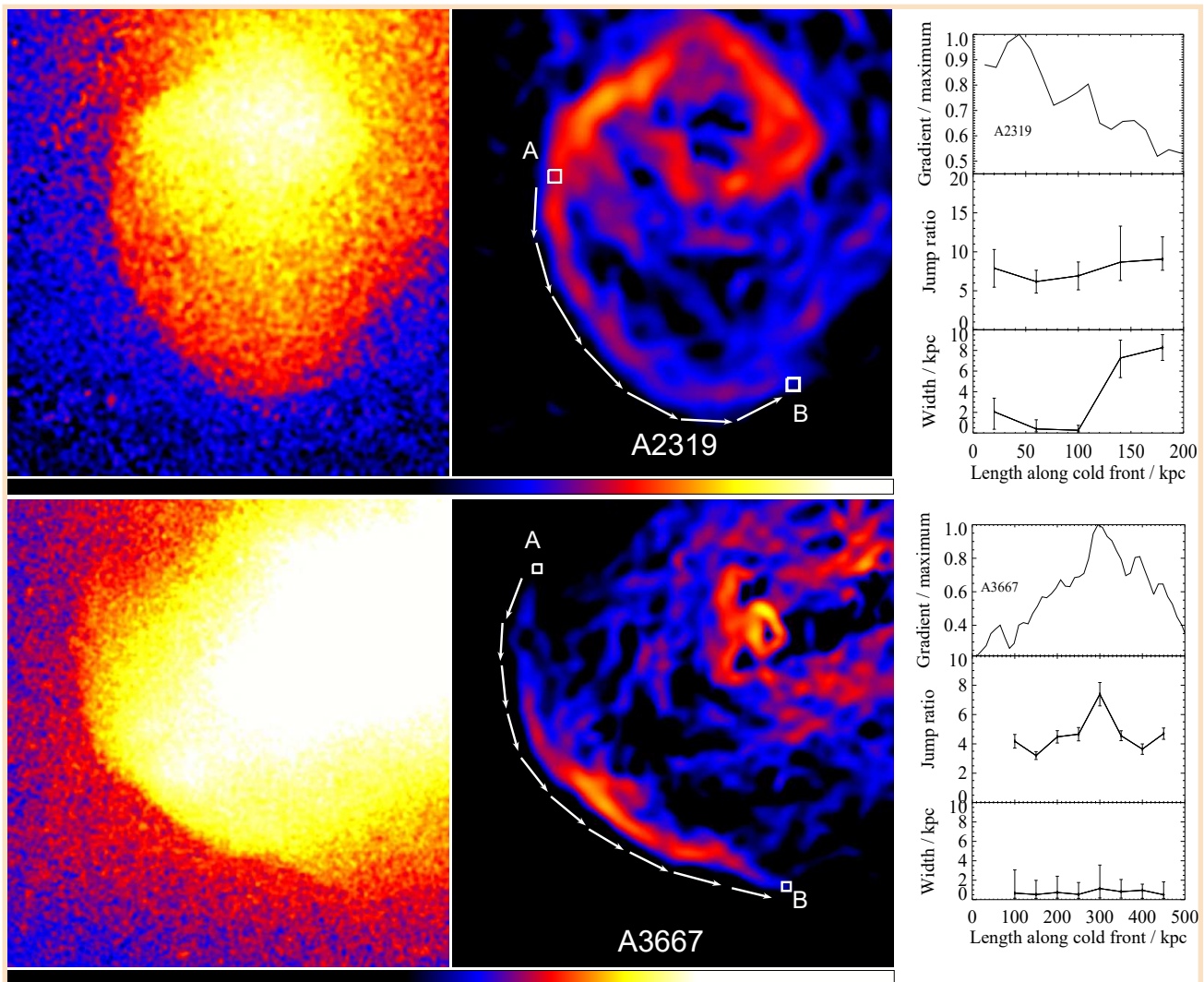


Figure 6. Looking at gradient variations along the lengths of the cold fronts in A2319 (top row) and A3667 (bottom row). On the left is the initial *Chandra* image, in the middle is the GGM filtered image, and on the right are the variations of the GGM magnitude, the jump ratio and the cold front width along the lengths of the fronts from position A to position B. Adapted from Walker et al. (2016).

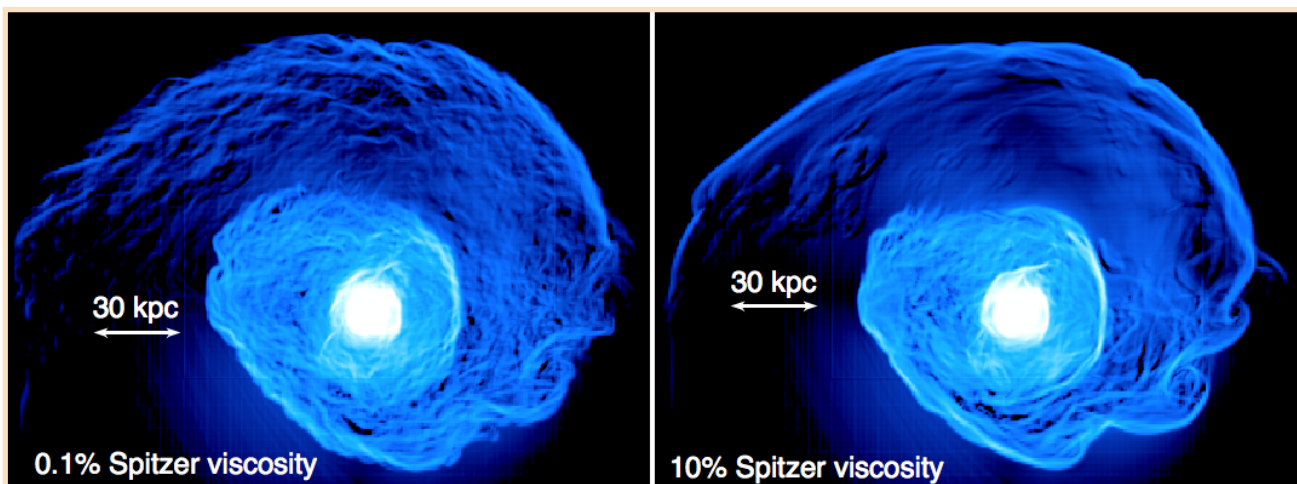


Figure 7: Sobel-filtered images of X-ray surface brightness from simulations of the Virgo cluster with varying viscosity. Viscosity smooths out the large cold front edges and reduces the number of smaller edge features produced by turbulent gas motions under the fronts. Reproduced from Roediger et al. (2013).

ZuHone et al. (2015) presented simulations of the Virgo cluster with varying viscosities and magnetic field strengths, and determined that a variety of the models for viscosity and moderately strong magnetic fields could result in cold fronts with similar appearance. This points to the main difficulty with using analysis of KHI at cold front surfaces alone to distinguish between the effects of these two distinct properties of the ICM, and suggests that other properties of the cluster gas should be examined to potentially break this degeneracy.

As previously noted, Roediger et al. (2013) used a Sobel filter to analyze images of X-ray surface brightness produced from simulations of the Virgo cluster (Figure 7). They examined hydrodynamic simulations with varying strengths of viscosity, and noted two distinguishing features in the filtered images. In the more viscous simulation, the cold front is a sharp continuous arc, whereas in the less viscous simulation it is distorted. Secondly, the filtered image revealed a wealth of structure in the low-viscosity simulation, produced by the undamped turbulent flow underneath the front surfaces.

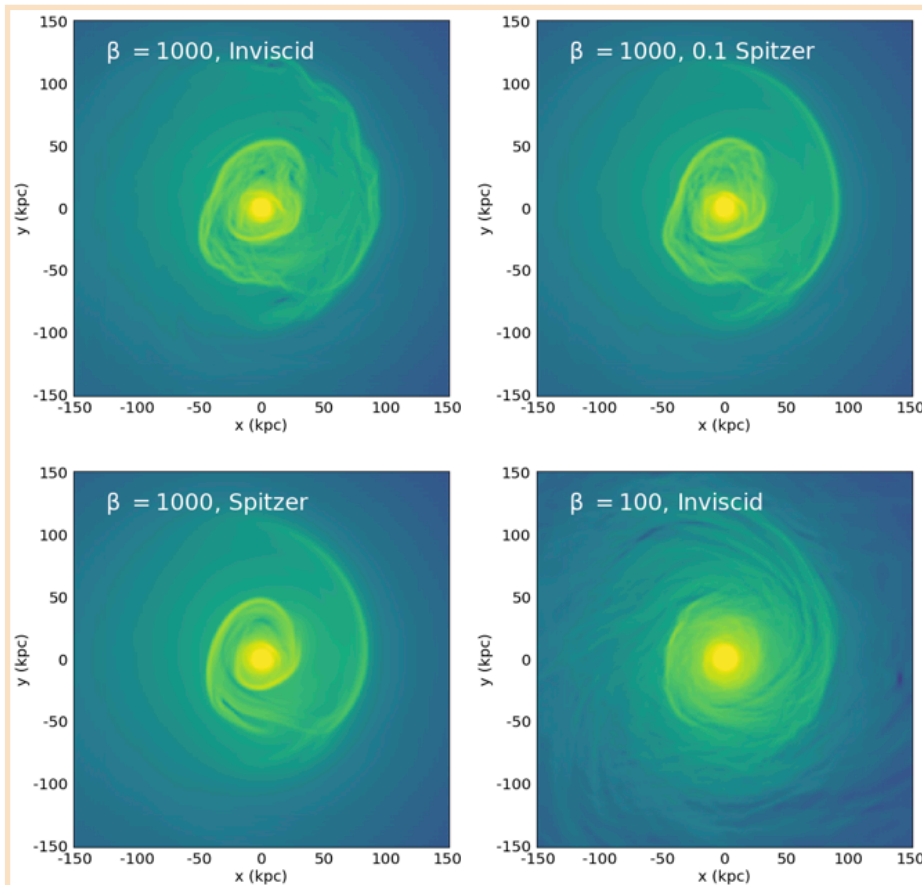


Figure 8: GGM-filtered images of X-ray surface brightness from four simulations from ZuHone et al. (2015), with varying magnetic field strength parameterized by the plasma  $\beta$  parameter and variations in viscosity given as a fraction of the *Spitzer* value given the local plasma properties. Increasing viscosity smooths out cold fronts and small-scale fluctuations, whereas increasing the magnetic field smooths out cold fronts but stretches fluctuations perpendicular to cold fronts, producing a banded structure underneath the front (Bellomi et al. 2018, in preparation).

Bellomi et al. (2018, in preparation) performs a similar analysis using the GGM filter on simulated X-ray images of cold fronts in a galaxy cluster core from the MHD simulations from ZuHone et al. (2015), who simulated a parameter space over magnetic field strength and viscosity. They confirm that increasing the viscosity smooths out the cold fronts and reduces smaller-scale edge features produced by the turbulence, which is damped out by higher viscosity (top-left, top-right, and bottom-left panels of Figure 8). In the case of an increased magnetic field (parameterized by the plasma  $\beta$  parameter, which is the ratio of the thermal to the magnetic pressures), though the cold fronts are indeed smoothed out, the edge structures underneath the front remain, but with a distinctly different character. The stretched and amplified magnetic field under the front produces long, band-like edge structures which vary in surface brightness primarily along the radial direction, correlating with small variations in the magnetic field strength. These very different signatures in surface brightness provide a potential opportunity to distinguish between the two ICM

properties of viscosity and magnetic field strength.

The primary challenge in discerning plasma properties such as these from edge-filtered images from real observations is that of statistics. As noted above, not all structures seen in the images are physical—the small-scale “wormy” features in particular are artifacts of the Poisson noise inherent in the X-ray images. Thus, definitively distinguishing between the different physical processes operating in the ICM as demonstrated above in the noiseless simulated images would require a very high signal-to-noise ratio in addition to high spatial resolution. Given the decrease of the low-energy response of *Chandra*/ACIS, such an analysis is likely out of its grasp (with the possible exception of the Perseus cluster), but would be well within the capabilities of *Lynx* (see Figure 9). Future work using realistic mock X-ray observations of simulated clusters will determine what observational capabilities would be required to use this technique to further elucidate the plasma physics of the ICM. ■

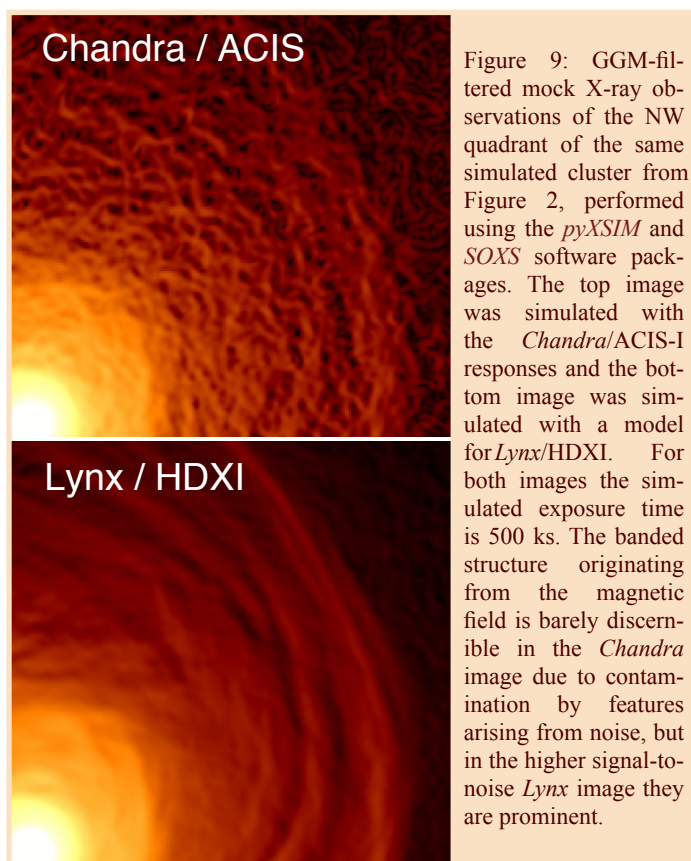


Figure 9: GGM-filtered mock X-ray observations of the NW quadrant of the same simulated cluster from Figure 2, performed using the *pyXSIM* and *SOXS* software packages. The top image was simulated with the *Chandra/ACIS-I* responses and the bottom image was simulated with a model for *Lynx/HDXI*. For both images the simulated exposure time is 500 ks. The banded structure originating from the magnetic field is barely discernible in the *Chandra* image due to contamination by features arising from noise, but in the higher signal-to-noise *Lynx* image they are prominent.

## REFERENCES

- Fabian A.C. Sanders J.S., Allen S.W., Crawford C.S., Iwasawa K., Johnstone R.M., Schmidt R.W., Taylor G.B., MNRAS, 2003, 344, L43
- Forman W., et al., 2007, ApJ, 665, 1057
- Grebenev S.A., Forman W., Jones C., Murray S., 1995, 445, 607
- Laing R.A., Bridle A.H., 2013, MNRAS, 432, 1114
- Malin D.F., Zealey W.J., 1979, Sky and Telescope, 57, 354
- Markevitch M., Vikhlinin A., 2007, Physics Reports, 443, 1
- Marshall H. L., Miller B. P., Davis D. S., Perlman E. S., Wise M., Canizares C. R., Harris D. E., 2002, ApJ, 564, 683
- Roediger E., Bruggen M., Simionescu A., Bohringer H., Churazov E., Forman W. R., 2011, MNRAS, 413, 2057
- Roediger E., Kraft R. P., Forman W. R., Nulsen P. E. J., Churazov E., 2013, ApJ, 764, 60
- Sanders J.S., Fabian A.C., 2002, MNRAS, 331, 273
- Sanders J.S., Fabian A.C., 2008, MNRAS, 390, L93
- Sanders J.S., Fabian A.C., Taylor G.B., Russell H.R., Blundell K.M., Canning, R.E.A., Hlavacek-Larrondo J., Walker S.A., Grimes C.K., MNRAS, 2016a, 457, 82
- Sanders J.S., Fabian A.C., Russell H.R., Walker S.A., Blundell K.M., MNRAS, 2016b, 460, 1898
- Sanders J.S., Fabian A.C., Russell H.R., Walker S.A., 2018, MNRAS, 474, 1065
- Walker S. A., Sanders J. S., Fabian A. C., 2016, MNRAS, 461, 684
- Walker, S. A., Hlavacek-Larrondo, J., Gendron-Marsolais, M., et al., 2017, MNRAS, 468, 2506
- Young A. J., Wilson A. S., Mundell C. G., 2002, ApJ, 579, 560
- ZuHone J. A., Markevitch M., Lee D., 2011, ApJ, 743, 16
- ZuHone, J. A., Kunz, M. W., Markevitch, M., Stone, J. M., & Biffi, V. 2015, ApJ, 798, 90
- ZuHone J.A., Kowalik K., Ohman E., Lau E., Nagai, D. 2018, ApJS 234, 4